Notice of Copyright:

This manuscript has been co-authored by UT-Battelle, LLC, under contract DE-AC05-00OR22725 with the US Department of Energy (DOE). The US government retains and the publisher, by accepting the article for publication, acknowledges that the US government retains a nonexclusive, paid-up, irrevocable, worldwide license to publish or reproduce the published form of this manuscript, or allow others to do so, for US government purposes. DOE will provide public access to these results of federally sponsored research in accordance with the DOE Public Access Plan (http://energy.gov/downloads/doe-public-access-plan).

Potentials with Small-Angle Neutron Scattering Technique for Understanding Structure-Property Relation of 3D-Printed Materials

*Tae Hui Kang[1], Brett G. Compton[2], William T. Heller[1], Shuo Qian[1], Gregory S. Smith[1], Volker S. Urban[1], Chad E. Duty[2,3], and Changwoo Do[1, *]*

[1] Neutron Scattering Division, Oak Ridge National Laboratory, Oak Ridge, TN 37831, USA

[2] Department of Mechanical, Aerospace and Biomedical Engineering, University of Tennessee, Knoxville, TN 37996, USA

[3] Manufacturing Demonstration Facility, Oak Ridge National Laboratory, Oak Ridge, TN 37831, USAAUTHOR INFORMATION

Corresponding Author

* Changwoo Do, doc1@ornl.gov

ABSTRACT

Carbon fiber (CF)-embedded acrylonitrile butadiene styrene polymer composites printed on the large-scale printer at Oak Ridge National Laboratory were investigated by small-angle neutron scattering to correlate the microstructure of the composites with their mechanical strength. The microstructure of the polymer domains and the alignment of CF were characterized across the interfaces between layers of the hot-melt extruded material and were compared to CF-free ABS. The SANS data show that the CF-containing material displays strong anisotropic scatterings suggesting molecular alignment along the printing direction that is not present in the CF-free ABS. Scattering data analysis across the interfacial layer revealed enhanced molecular alignment along the printing direction near the boundaries and inhomogeneous size distribution of polymer domains upon the addition of CF. We attribute the compromised strength across interfacial layers from CF-containing material to this inhomogeneous size distribution which prevents effective lateral interaction between layers.

Ⅰ. INTRODUCTION

Additive manufacturing technologies are widely utilized to fabricate 3D-objects for diverse applications, such as nanofabrication, matrices for human cell culture growth, and custom reaction ware for chemical synthesis [1–3]. While existing printing technology such as the hot-melt extrusion process has shown great potentials for the fabrication of large and complex 3D-objects [4,5] such as the 3D-printed Shelby Cobra vehicle by Manufacturing Demonstration Facility, Oak ridge National Laboratory, achieving materials properties comparable to the ones made by conventional polymer processing remains a big challenge. One of the critical issues in creating large-scale printed object is to have strong enough mechanical strength of the materials so that the large structure can withstand its heavy load. For this purpose, polymer composites are frequently considered in wide ranges of 3D printed objects.

In polymer composites, the distribution and orientation of the filler materials play critical roles in defining the properties of the composites. For example, the degree of dispersion of nanoparticles in polymer composites is known to be critical for producing functional films, coatings, and membranes [6–8]. The orientation of anisotropic filler particles such as clay platelets and their interaction with polymers [9] also affect the rheological properties of polymer melts [10,11]. As a result, diverse filler materials such as carbon fiber, glass fiber, silica, and clay nano-platelets have been considered for enhancing various physical properties of 3D-printed objects, such as the strength, stiffness, and thermal conductivity [12–15].

Although the addition of fillers to polymers can enhance material properties in bulk, similar composition has not lead to major improvements in 3D printed materials so far [15,16]. Even though material properties in the extrusion direction are improved, the layer-layer adhesion is appeared to be negatively affected by the addition of filler materials. The delamination (i.e. the

separation between adjacent layers) problem is especially critical for the wide-spread adoption of large, mass produced 3D-printed objects [17]. Efforts are being made to understand sources for the delamination problem. For examples, molecular simulations showed that the molecule alignment of an amorphous polymer melt in the flow results in disentanglement of polymer chain near the layer interface, which may lead to de-bonding of the extruded layers [18]. In the case of 3D-printed polymer composites, the presence of filler materials, such as carbon fibers, was reported to introduce pores around the fibers, which lead to weaker fiber bonding to polymer matrix, causing a decrease in the mechanical strength of the objects [19]. These studies suggest that the presence of filler materials alters the polymer chain conformation as well as bulk properties in the extruded polymer melt during the printing process in a manner that negatively influences the structure of the material at the interfaces between deposited layers.

To understand how the filler influences the structure of polymer materials in 3D-printed polymer composites, the effect of CF on 3D-printed polymers such as acrylonitrile butadiene styrene (ABS) was studied by small-angle neutron scattering (SANS) [20]. Small angle scattering technique is an ideal tool to probe nm-scale microstructures that are relevant to the conformation of polymer chains and domains. In order to preserve the material's bulk mechanical properties for the scattering experiments, printed objects cannot be sliced too thin. Therefore, neutron's strong penetration power is highly desired in performing ex-situ measurements on relatively thick (1mm) specimen, which is critical in correlating microstructure with mechanical properties. Here, we attempt to provide experimental evidences correlating molecular level structures with the material's mechanical properties by spatially-resolved SANS measurements on 3D printed samples. The microstructure of the printed materials across the layer-layer interfaces have been mapped out at spatial resolution of 1 mm.

Ⅱ. Experimental

A. Materials

Samples prepared for SANS characterization were taken from thin-walled sections of components printed on the Big Area Additive Manufacturing (BAAM-CI) 3D-printing platform developed at Oak Ridge National Laboratory in collaboration with Cincinnati Incorporated. BAAM-CI uses pelletized thermoplastic feedstock, similar to that used for injection molding, and can deposit up to 50 kg (~40000 cm^3) of material per hour over a build area of 3 × 6 × 2 m. For this study, two feedstock materials were used: neat ABS (product Techmer 5 MFI High Impact ABS) and 20-weight-% (wt%) carbon fiber (7 μm in diameter; ~100 μm mean length)-reinforced ABS (product Techmer Electrafil J-1200/CF/20) supplied by Techmer PM (Clinton, TN). Thin walls (20 mm thick) comprising two ~10-mm-thick beads were deposited at 250 °C with a 7.6 mm-diameter nozzle at a translation speed of 254 mm/s. Individual samples were then rough cut on a bandsaw and ground to ~1 mm thickness using a standard belt sander. Care was taken to ensure that the sample comprised the central portion of the deposited beads.

B. Mechanical property measurement

Mechanical strength data were measured for printed neat ABS and 20 wt% CF-containing ABS composite using tensile test specimens that were water-jet-cut from 25-mm-thick printed walls or plates in the X-, Y-, and Z-directions, corresponding to longitudinal, transverse and out-of-plane loading directions (Fig. 1). Tensile tests were conducted according to ASTM D638. The full mechanical analysis is presented elsewhere [21].

C. Small-Angle Neutron Scattering

The schematic of the SANS experiment is shown in Fig. 1. The 3D-printed ABS composites by the BAAM-CI system were cut with 1 mm thickness at the X-Y plane for the SANS experiment, and the cutting section was scanned along a 24 mm strip in the horizontal direction, X (FIG. 1). SANS measurements were performed at the EQ-SANS instrument at the Spallation Neutron Source (SNS) located at Oak Ridge National Laboratory (ORNL) using 60 Hz operation mode. The sample-to-detector distances of 4 m and 4.5 m were used with minimum wavelength of 2.5A, covering a Q range of 0.015 $Å^{-1} < Q < 0.3$ $Å^{-1}$ where $Q = (4\pi/\lambda) \sin(\theta/2)$ is the magnitude of the scattering vector, and θ is the scattering angle. The incident beam was collimated using a sample aperture of 1 and 2 mm. The measured scattering intensity was corrected according to standard procedures with Mantid Plot [22], and the reduced intensities were placed on an absolute scale using a calibrated standard porous silica. All SANS measurements were performed at ambient temperature (~20 ˚C).

The printed ABS/CF sample is shown in Fig. 2. The boundaries were identified by visual inspection using an optical microscope based on the fine-scale porosity and different texture. And these boundaries between the extruded beads are highlighted as the vertical blue lines. The width of the visually identified layer has been indicated as well, and the inset image is a magnification of the area enclosed in the red box. Here, the interface layers are marked with dashed lines and the bands of more highly aligned fibers are visible near the layer interfaces. The horizontal arrow indicates the direction of the scan performed using the 1 mm diameter neutron beam.

Ⅲ. Results and Discussions

The mechanical properties of the 3D-printed polymer composites measured in the direction aligned with the deposition (Y) as well as across interfaces (X) have been measured [21]. (Table 1) The mechanical properties taken from typical, commercially-available injection molded samples by Techmer PM (Clinton, TN) are also provided for comparison with the materials produced by the BAAM-CI system. The 3D-printed ABS possesses 85% of the tensile strength of the reference material (42.1 MPa) in the deposition direction (Y, 35.6 MPa) and 63% in the cross-layer direction (X, 26.5 MPa). In contrast, the ABS/CF composite is much stronger along the printed direction (Y, 66.4 MPa), but it loses almost 89% of strength in the perpendicular direction (X, 10.3 MPa) compared to the injection molded reference (96.5 MPa). The degree of anisotropy for both the stiffness and the strength has been observed previously for CF-reinforced 3D-printed material and was attributed to the alignment of the CF that occurs during the deposition process [16,19]. The strain at failure is significantly reduced in both directions by the presence of CF.

The cross section of each material is first examined by using optical microscope (Fig. 3). The neat 3D-printed ABS (Fig. 3a) shows that the printed beads are well blended with neighboring beads compared to the 3D-printed ABS/CF composite (Fig. 3b). The size of printed bead is clearly noticeable from the cross section of 3D-printed ABS/CF composites; the dark regions and lines show boundaries of the individual bead, which are the macroscopic evidence of delamination. The grainy appearance of the individual ABS/CF bead indicates the existence of the intra-bead voids around fillers. These voids observed from 3D printed ABS/CF composites are consistent with the voids found in the fiber composites by Tekinalp and co-workers [19]. It is possible that the formation of inter-layer entanglement is influenced by the distribution and orientation of the filler

materials. Therefore, we have performed SANS experiments to understanding the role of the filler material and elucidate the problem with delamination.

The scattering contrast from the neat ABS polymer comes from the scattering length density (SLD) contrast between the acrylonitrile-styrene and butadiene regions, which can be described as density fluctuation of inhomogeneous polymer domains. (Table 2) Isotropic 2D scattering profile of the 3D printed ABS only sample (Fig. 4a) indicates that there exists no microscopic level deformation or orientation of polymer domains. On the other hand, anisotropic scattering pattern is observed from the 3D printed ABS composite with filler particles (CF). (Fig. 4b) This is indicative of microscopic alignment of polymers or filler materials inside ABS/CF composite. The scattering intensities at different Q values (dQ = 0.03 Å^{-1}) have been plotted as a function of the azimuthal angle ϕ for the estimation of degree of anisotropy. (Fig. 4c, 4d) While scattering intensities from the printed neat ABS are uniform in the azimuthal angle ϕ, the scattering intensities from the ABS/CF composite peak around ± 90˚, which is perpendicular to the printing direction. This is strong indication of preferential spatial alignment of molecules along the direction of the printing flow. In our ABS/CF composite, the scattering intensities can be contributed by either the scattering contrast between different domains of ABS polymers or the scattering contrast between ABS polymer and CF (SLD = 5.5 × 10^{-6} Å^{-2} [23]). Therefore, it is likely that both components (ABS and CF) have developed alignment along the printing direction during the extrusion from the nozzle as reported by others [18, 24]. It is also observed that this anisotropic scattering is significantly reduced and disappear as the Q increases, indicating that the material becomes more uniform at the length scale of individual polymer segment. To investigate the structural changes at the interface between printed layers, SANS data were collected from the 3D-

printed ABS/CF composite at several positions along a 24 mm strip in the horizontal direction, X, at 1 mm intervals.

In order to quantitatively compare the degree of anisotropy in bulk and delamination regions, the order parameter, P_2, has been determined at different positions along the horizontal direction with 1 mm step. The order parameter is calculated by integrating the scattering intensity over the azimuthal angle ϕ from -180˚ to 180˚ and defined as [25,26]

$$P_2 = \frac{3 < \cos^2 \emptyset > -1}{2} \quad (2)$$

with

$$< \cos^2 \emptyset > \; = \frac{\int_{-\pi}^{\pi} (I_Q(\emptyset) \cos^2 \emptyset |\sin \emptyset|) d\emptyset}{\int_{-\pi}^{\pi} (I_Q(\emptyset) |\sin \emptyset|) d\emptyset} \quad (3).$$

The order parameter defined in Eq. 2 has theoretical limiting values of 1 and -0.5 for systems with ideal alignment along the $\emptyset$ = 0^o and 90^o, respectively. Isotropic distribution of orientation will have P_2 = 0. The order parameter of the ABS/CF composite was estimated for different positions along the X-direction (Fig. 5). Interestingly, a periodicity of ~4 mm width could be identified, which is consistent with the map of the sample shown in Fig. 2. The order parameter is close to zero with increasing Q, confirming that the material has isotropic distribution of orientation when viewed at shorter length scales.

As shown in Fig. 5, the order parameter of the ABS/CF ranges from -0.12 to -0.06 at Q = 0.045 Å^{-1}. Smaller value of the order parameter indicates better alignment to the printing direction. For the printed neat ABS, the order parameter at Q = 0.045 Å^{-1} is -0.004 (taken at X = 6 mm but similar for all X values), which is higher than the maximum value of printed ABS/CF, -0.06, indicating negligible alignment using neat ABS. The value and periodicity of P_2 in the ABS/CF strongly suggests that the alignment of CF and polymers around it is position sensitive and the

alignment is stronger at the delamination layers in the sample. For extrusion printing, this is understandable because both polymers and particles have shown enhanced stretching and ordering near the wall due to the higher shear rate [18, 27]. We propose that a similar physical mechanism produces the molecular alignment near the layer interface than bulk region (in the middle of the polymer bead) due to the enhanced shear-strain rate induced by the flow of polymer melt at the nozzle.

A correlation length of the polymer domain can describe rough characteristics of the structure of polymers. For a non-particulate two-phase system, DAB (Debye-Anderson-Brumberger) model can be used to characterize the polymer domain structure and understand the influence of added filler materials. The model is described by a correlation length (ξ), which is the average spacing between the acrylonitrile-styrene and butadiene regions [28,29].

$$I(Q) = \frac{D\xi^3}{(1 + (Q\xi)^2)^2} \quad (4)$$

The scale factor, D, is related to the volume fraction of the two phases, φ_1 and φ_2, and their scattering length density contrast, $\Delta\rho$, via

$$D = 8\pi(\Delta\rho)^2\varphi_1\varphi_2 \quad (5)$$

To apply the DAB model for fitting, the 2D scattering profiles of the 3D-printed polymer composite were averaged azimuthally. For an anisotropic scattering profile, two 1D scattering intensities were obtained by averaging in $\Delta Ø = 10^\circ$ sectors perpendicular (Q_x) and parallel (Q_y) to the printing direction respectively, to characterize the local structure in horizontal and vertical directions separately. The orientation of peaks around ± 90˚ shown in Fig. 4d is perpendicular to the printing direction. A closer look at the orientation of peaks shows position dependent fluctuation around ± 90˚ due to the macroscopic orientation variation of the deposited polymer layer, which is intrinsically imperfect in the 3D printing method. (Fig. 2) Therefore, the orientation

of the peak is used as a reference of the azimuthal angle to define perpendicular and parallel component of the anisotropic scattering profile. (Supplementary material)

These one-dimensional scattering profiles are summarized in Fig. 6a. The DAB model was used to fit an averaged scattering profile of ABS/CF composite in Q_y and circular-averaged scattering profile of ABS reasonably well. An averaged scattering profile of ABS/CF composite in Q_x could not be fitted well by Eq. 4, because of the scattering features above Q = 0.04 Å^{-1} that is indicative of structure of a few tens of angstrom. Therefore, we used the DAB model with two characteristic lengths, ξ and Ξ, as below to fit the scattering profile in Q_x.

$$I(Q_x) = \frac{D_1\xi^3}{\left(1 + (Q_x\xi)^2\right)^2} + \frac{D_2\Xi^3}{\left(1 + (Q_x\Xi)^2\right)^2} \quad (6)$$

The correlation length obtained from the data fitting is summarized in Fig. 6b. At given Q range, we assumed that the scattering contribution from CF is negligible compared to the scattering contributions from ABS domains, because the mean length of CF is a few hundred micrometer which is far outside the measured Q ranges (see the supplementary material for detailed discussion on the theoretically calculated scattering profiles by model systems). The correlation length, ξ, from the ABS/CF composite shows fluctuation along the scanning position (X), while the correlation length of the neat ABS is featureless and independent of the position. This reveals that the size of polymer domains is not evenly distributed when CF is added. The inhomogeneous polymer domain can potentially play a role in the interaction between printed layers resulting in the compromised strength across interfaces, even though the mechanical strength along the extrusion direction is generally enhanced due to the alignment of CF. The second correlation length, Ξ, is obtained to be order of a few Å, which is much smaller than the primary correlation length, ξ. It is possible that the second length scale may come from the confined polymers among the CFs [30]. However, it is difficult to provide definitive answers to the origin of the small

correlation length without further experiments, which can be a follow-up investigation with deuterated polymers.

Ⅳ. CONCLUSIONS

The alignment of CF and the microstructure of polymer domains in the 3D-printed ABS composite were investigated using SANS. The anisotropic scattering profiles which is indicative of alignment of materials along the printing deposition direction were only observed in the ABS/CF composites. The degree of alignment was measured to be slightly stronger near the interfaces than in the middle of the beads. In the presence of CF, the distribution of correlation length of the polymer domain becomes inhomogeneous across the printing layers, which may lead to the weak lateral interaction between neighboring layers. These experimental observations show strong potentials of SANS investigations in revealing correlation between microstructure of polymer domains and the mechanical property of the printed object. Future SANS experiments with deuterated polymers are expected to provide more definitive answers to questions regarding to the origins of correlation lengths and the chain conformation as a function of position.

SUPPLEMENTARY MATERIAL

See supplementary material for the position-dependent scattering data of the ABS/CF composite; theoretically calculated scattering profiles by model systems.

ACKNOWLEDGEMENTS

The Research was sponsored by the U.S. Department of Energy, Office of Energy Efficiency and Renewable Energy, Advanced Manufacturing Office, under contract DE-AC05-00OR22725 with UT-Battelle, LLC. The Research at Oak Ridge National Laboratory's Spallation Neutron

Source was sponsored by the Scientific User Facilities Division, Office of Basic Energy Sciences, U.S. Department of Energy. Research presented in this work was also supported by the Laboratory Directed Research and Development Program (LDRD-7641) of Oak Ridge National Laboratory, managed by UT-Battelle, LLC, for the U. S. Department of Energy. Notice: This manuscript has been authored by UT-Battelle, LLC under Contract No. DE-AC05-00OR22725 with the U.S. Department of Energy. The United States Government retains and the publisher, by accepting the article for publication, acknowledges that the United States Government retains a non-exclusive, paid-up, irrevocable, world-wide license to publish or reproduce the published form of this manuscript, or allow others to do so, for United States Government purposes. The Department of Energy will provide public access to these results of federally sponsored research in accordance with the DOE Public Access Plan (http://energy.gov/downloads/doe-public-access-plan). The authors thank Dr. Wim Bras for scientific advices.

References

1. N. Jones, Nature, **487**, 22 (2012).

2. M.D. Symes, P.J. Kitson, J. Yan, C.J. Richmond, G.J.T. Cooper, R.W. Bowman, T. Vilbrandt, and L. Cronin, Nat. Chem., **4**, 349 (2012).

3. M. Vaezi, H. Seitz, and S. Yang, Int. J. Adv. Manuf. Technol., **67**, 1721 (2013).

4. Z. Quan, Z. Larimore, A. Wu, J. Yu, X. Qin, M. Mirotznik, J. Suhr, J.-H. Byun, Y. Oh, and T.-W. Chou, Compos. Sci. Technol., **126**, 139 (2016).

5. Z. Quan, Z. Larimore, X. Qin, J. Yu, M. Mirotznik, J.-H. Byun, Y. Oh, and T.-W. Chou, Compos. Sci. Technol., **131**, 48 (2016).

6. M.J. Percy, J.I. Amalvy, C. Barthet, S.P. Armes, S.J. Greaves, J.F. Watts, and H. Wiese, J. Mater. Chem., **12**, 697 (2002).

7. J.I. Amalvy, M.J. Percy, S.P. Armes, and H. Wiese, Langmuir, **17**, 4770 (2001).

8. A.J. Merkel, T. C.; Freeman, B. D.; Spontak, R. J.; He, Z.; Pinnau, I.; Meakin, P.; Hill, Science, **296**, 519 (2002).

9. P.F. Luckham and S. Rossi, Adv. Colloid Interface Sci., **82**, 43 (1999).

10 S. Pujari, L. Dougherty, C. Mobuchon, P.J. Carreau, M.-C. Heuzey, and W.R. Burghardt, Rheol. Acta, **50**, 3 (2011).

11. L.M.C. Dykes, J.M. Torkelson, W.R. Burghardt, and R. Krishnamoorti, Polymer, **51**, 4916 (2010).

12. P. Calvert and R. Crockett, Chem. Mater., **9**, 650 (1997).

13. Y.T. Vu, J.E. Mark, L.H. Pham, and M. Engelhardt, J. Appl. Polym. Sci., **82**, 1391 (2001).

14. G. Mathew, M.-Y. Huh, J.M. Rhee, M.-H. Lee, and C. Nah, Polym. Adv. Technol., **15**, 400 (2004).

15. L.J. Love, V. Kunc, O. Rios, C.E. Duty, A.M. Elliott, B.K. Post, R.J. Smith, and C.A. Blue, J. Mater. Res., **29**, 1893 (2014).

16. B.G. Compton and J.A. Lewis, Adv. Mater., **26**, 5930 (2014).

17. V. Vega, J. Clements, T. Lam, A. Abad, B. Fritz, N. Ula, and O.S. Es-Said, J. Mater. Eng. Perform., **20**, 978 (2011).

18. C. McIlroy and P.D. Olmsted, J. Rheol., **61**, 379 (2017).

19. H.L. Tekinalp, V. Kunc, G.M. Velez-Garcia, C.E. Duty, L.J. Love, A.K. Naskar, C.A. Blue, and S. Ozcan, Compos. Sci. Technol., **105**, 144 (2014).

20. S. Chand, J. Mater. Sci., **35**, 1303 (2000).

21. C. Duty, V. Kunc, B. Compton, B. Post, D. Erdman, R. Smith, R. Lind, P. Lloyd, and L. Love, Rapid Prototyp., J. **23**, 1 (2017).

22. O. Arnold, J.C. Bilheux, J.M. Borreguero, A. Buts, S.I. Campbell, L. Chapon, M. Doucet, N. Draper, R. Ferraz Leal, M.A. Gigg, V.E. Lynch, A. Markvardsen, D.J. Mikkelson, R.L. Mikkelson, R. Miller, K. Palmen, P. Parker, G. Passos, T.G. Perring, P.F. Peterson, S. Ren, M.A. Reuter, A.T. Savici, J.W. Taylor, R.J. Taylor, R. Tolchenov, W. Zhou, and J. Zikovsky, Nucl. Instruments Methods Phys. Res. Sect. A Accel. Spectrometers, Detect. Assoc. Equip., **764**, 156 (2014).

23. E. Hoinkis and M. Ziehl, Carbon, **41**, 2047 (2003).

24. S.J.S. Qazi, A.R. Rennie, and J.K. Cockcroft, Langmuir, **28**, 3704 (2012).

25. A. Böker, H. Elbs, H. Hänsel, A. Knoll, S. Ludwigs, H. Zettl, A. V. Zvelindovsky, G.J.A. Sevink, V. Urban, V. Abetz, A.H.E. Müller, and G. Krausch, Macromolecules, **36**, 8078 (2003).

26. S.J.S. Qazi, A.R. Rennie, I. Tucker, J. Penfold, and I. Grillo, J. Phys. Chem. B, **115**, 3271 (2011).

27. S.J.S. Qazi, A.R. Rennie, J.P. Wright, and J.K. Cockcroft, Langmuir, **26**, 18701 (2010).

28. P. Debye, H.R. Anderson, and H. Brumberger, J. Appl. Phys., **28**, 679 (1957).

29. P. Debye and A.M. Bueche, J. Appl. Phys., **20**, 518 (1949).

30. Y. Wang and I. Teraoka, Macromolecules, **33**, 3478 (2000).

TABLE 1. Mechanical properties of 3D-printed ABS and ABS/CF composite. For the definition of X and Y, see Fig. 1.

Materials	Strength (MPa)	Stiffness (GPa)	Strain (%)
3D-printed ABS[a]			
X	26.5	2.21	1.39
	± 3.3	± 0.02	± 0.08
Y	35.6	2.32	3.07
	± 0.5	± 0.09	± 0.86
Injection-molded ABS[b]	42.1	2.55	
3D-printed ABS/CF[a]			
X	10.3	2.13	0.55
	± 1.3	± 0.08	± 0.13
Y	66.4	11.94	0.65
	± 0.7	± 0.54	± 0.03
Injection-molded ABS/CF[b]	96.5	12.41	

[a]Tensile strength, stiffness, and percent elongation strain of 3D-printed ABS and ABS/CF composite by the BAAM-CI system [21].

[b]The mechanical properties taken from typical injection molded samples by Techmer PM are summarized for comparison.

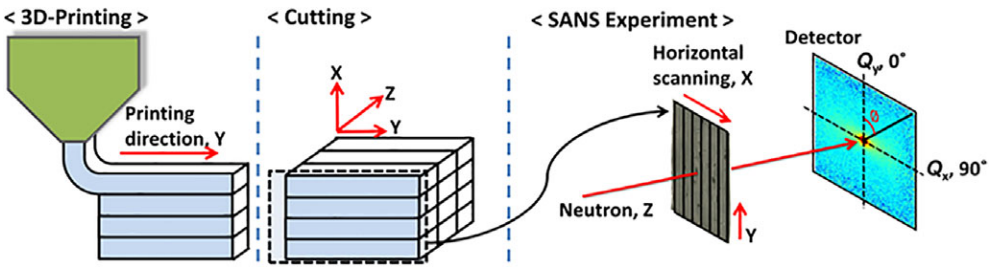

Figure 1. Schematic of 3D-printing, cutting, and SANS experiment.

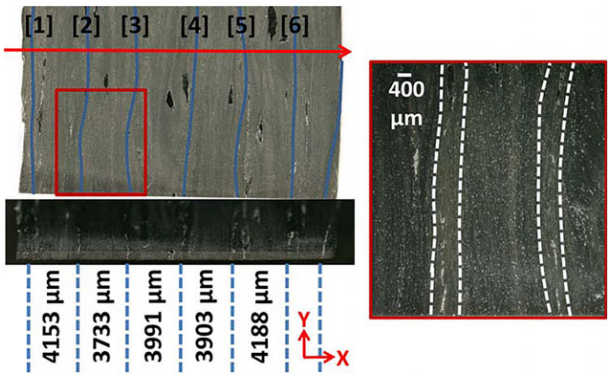

Figure 2. Microstructure image of the 3D-printed ABS/CF composite. The identified layer boundaries on the ABS/CF composite are highlighted as the vertical blue lines, and the width of the extruded beads represent. The axes of the horizontal scanning direction X and the printing direction Y are indicated, and the boundaries are numbered for convenience. SANS experiment was performed along the red horizontal line using the 1 mm diameter beam. And a magnification of the area enclosed in the red box is shown in the inset image.

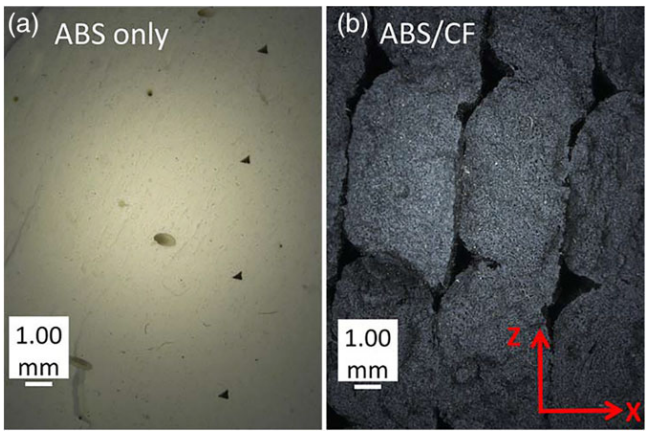

Figure 3. Fracture surface images of 3D-printed (a) ABS and (b) ABS/CF composite. The axes of surface plane, the horizontal scanning direction X and the out-of-plane Z, are indicated.

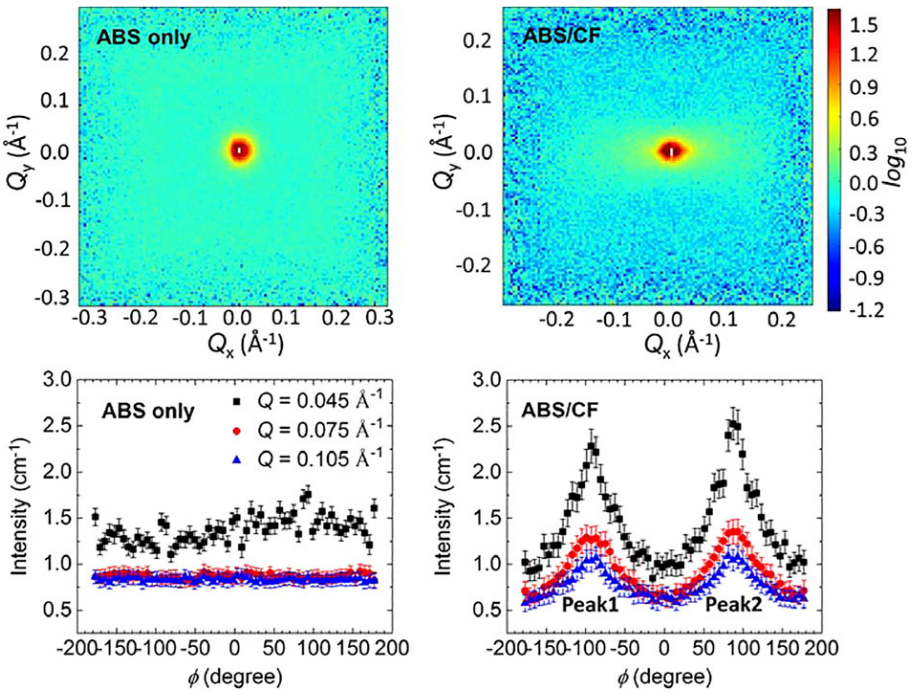

Figure 4. 2D scattering profiles from (a) neat ABS (X = 6 mm) and (b) ABS/CF composite (X = 5 mm). Azimuthal intensity distributions of (c) neat ABS (X = 6 mm) and (d) ABS/CF composite (X = 5 mm) at selected Q values as examples, Q = 0.045 Å^{-1} (black dots), 0.075 Å^{-1} (red dots), and 0.105 Å^{-1} (blue dots).

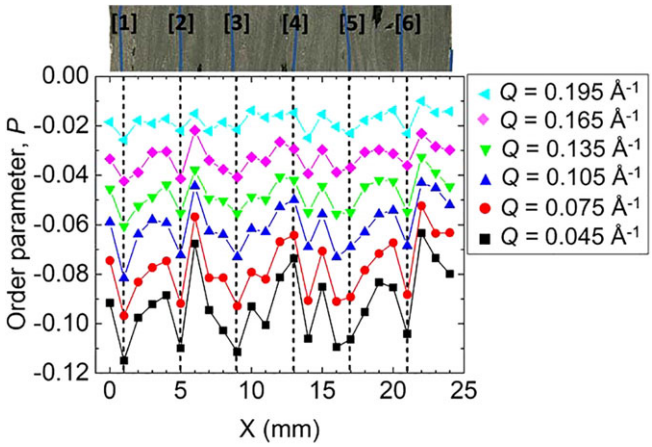

Figure 5. Position-dependent order parameter of ABS/CF composite in the range of Q from 0.045 $Å^{-1}$ to 0.195 $Å^{-1}$ (from bottom to top). The image of ABS/CF composite from FIG. 2 is shown on the top and the interface layers are marked with dashed lines.

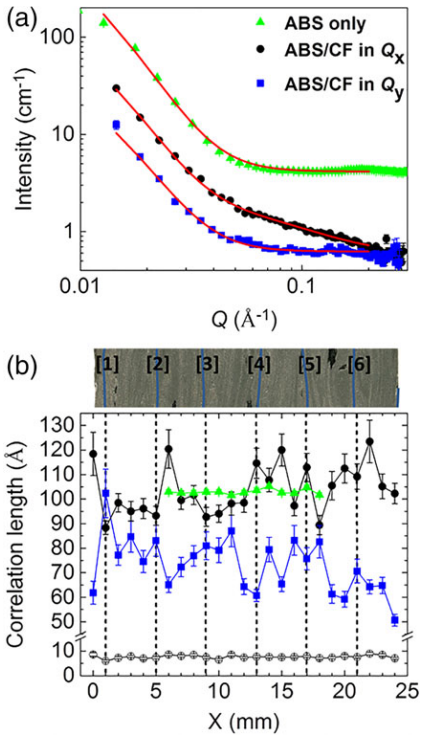

Figure 6. (a) Circular-averaged scattering profile of ABS (X = 6 mm) is shown with green dots. The averaged scattering profiles of ABS/CF composite in Q_x and Q_y at the position X = 5 mm are indicated black dots and blue dots, respectively. Each red line represents fitting curves by the DAB model. Scattering curve for the neat ABS has been shifted vertically for clarify. (b) Correlation length, ξ, obtained from the DAB model fits are summarized for neat ABS (green dots), ABS/CF composite in Q_x (black dots) and in Q_y (blue dots) along the horizontal position X. Correlation length, Ξ, for the ABS/CF composite in Q_x is shown with open black dots. Dashed line expresses the deposit layer interface of ABS/CF, and the position X for the neat ABS is not absolute position. The image of ABS/CF composite from Fig. 2 is shown above the plot.